Eur Biophys J (2004) 33: 130–139
DOI 10.1007/s00249-003-0360-5

ARTICLE

Michelle L. Gee · Levie Lensun · Trevor A. Smith
Colin A. Scholes

Time-resolved evanescent wave-induced fluorescence anisotropy for the determination of molecular conformational changes of proteins at an interface

Received: 21 March 2003 / Revised: 22 August 2003 / Accepted: 1 September 2003 / Published online: 28 October 2003

Abstract We have shown that the molecular conformation of a protein at an interface can be probed spatially using time-resolved evanescent wave-induced fluorescence spectroscopic (TREWIFS) techniques. Specifically, by varying the penetration depth of the evanescent field, variable-angle TREWIFS, coupled with variable-angle evanescent wave-induced time-resolved fluorescence anisotropy measurements, allow us to monitor how fluorescence intensity and fluorescence depolarization vary normal to an interface as a function of time after excitation. We have applied this technique to the study of bovine serum albumin (BSA) complexed noncovalently with the fluorophore 1-anilinonaphthalene-8-sulfonic acid. The fluorescence decay varies as a function of the penetration depth of the evanescent wave in a manner that indicates a gradient of hydrophobicity through the adsorbed protein, normal to the interface. Restriction of the fluorescent probe's motion also occurs as a function of distance normal to the interface. The results are consistent with a model of partial protein denaturation: at the surface, an adsorbed BSA molecule unfolds, thus optimizing protein–silica interactions and the number of points of attachment to the surface. Further away, normal to the surface, the protein molecule maintains its coiled structure.

Keywords Bovine serum albumin · Fluorescence depolarization · Fluorescence intensity · Protein conformation · Time-resolved evanescent wave-induced fluorescence spectroscopy

Submitted as a record of the 2002 Australian Biophysical Society meeting

M. L. Gee (✉) · L. Lensun · T. A. Smith · C. A. Scholes
School of Chemistry,
University of Melbourne, 3010 Parkville,
Victoria, Australia
E-mail: mlgee@unimelb.edu.au

Introduction

The study of macromolecular interactions and dynamics of adsorbed species at an interface is of great importance to the understanding of a variety of phenomena in biotechnology and biocompatibility (Cornelius and Brash 1999; Ratner 1989). In many biotechnological areas, protein–receptor interactions at an interface are an issue. In the area of biocompatibility, understanding protein structural dynamics on surfaces, with a view to the development of materials suitable for bodily implants, is of primary interest since protein adhesion can have an adverse affect on a wide range of biomedical devices and prosthetics, in some cases leading to surface-induced thrombosis (Ratner 1989). In both of these areas, the surface activity of the protein, i.e. how the protein interacts with the substrate, is central. Insight into this can be gleaned from studies of the conformational changes that a protein undergoes as a result of its interaction with a substrate.

Despite the importance of protein surface activity to many systems, little is known about surface-induced protein conformational changes. As a consequence, there has been increasing interest in the development of powerful methodologies to enhance and extend surface characterization to the molecular level. An attractive way to probe interfacial phenomena is through the utilization of total internal reflection-based spectroscopic methods in which the penetrating evanescent field is used to photo-excite an absorbing species placed within the penetrating field (Harrick 1967). Such techniques can be used at the interface between many phases (e.g. liquid/solid, liquid/liquid, solid/solid, etc.).

The basic principles behind evanescent wave spectroscopy are illustrated schematically in Fig. 1. When light transmitted in a medium of refractive index n_1 encounters a medium of lower refractive index n_2, two processes can occur: when the angle of incidence is less than the critical angle, θ_c, defined by Snell's law as $\theta_c = \sin^{-1}(n_2/n_1)$, refraction occurs. For angles of

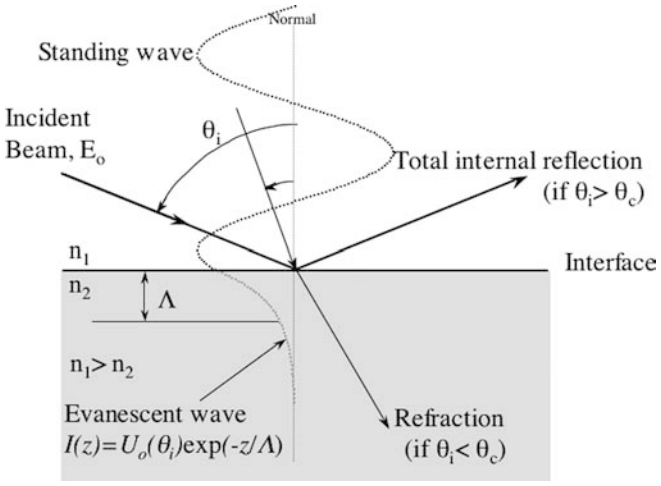

Fig. 1 Schematic representation of the total internal reflection (TIR) principle and the resulting standing evanescent wave. Λ is the penetration depth of the evanescent field (defined in text) which is related to the angle of incidence of the excitation light, θ_i, relative to the normal. z is the distance away from the interface

incidence greater than θ_c, total internal reflection (TIR) occurs. Maxwell's equations of electromagnetic radiation (Rumbles et al. 1991) predict that a small amount of the light field penetrates the lower refractive index medium in the form of a standing wave known as an evanescent wave. The intensity profile within the evanescent wave is related to the square of the E-field and decays exponentially with distance, z, from the interface, according to Eq. (1):

$$I(z) = U_0(\theta)\exp\left(\frac{-z}{\Lambda}\right) \tag{1}$$

where $U_0(\theta)\ \left(=E_0^2\right)$ is the intensity of the light at the interface, and the penetration depth, Λ, is defined as the distance into medium 2 normal to the interface at which the light intensity of the evanescent wave has decreased to 1/e of its interface value. Λ is related to the wavelength of the excitation radiation, λ, the angle of incidence, θ_i, the refractive index of medium 1, n_1, andthe critical angle for the pair of media, θ_c, through Eq. (2):

$$\Lambda = \frac{\lambda}{4\pi n_1}\frac{1}{\sqrt{\sin^2\theta_i - \sin^2\theta_c}} \tag{2}$$

TIR techniques can be extended to the fluorescence domain: if the absorbing species is also fluorescent, the evanescent field can induce fluorescence in the interfacial region, the intensity, I_f, of which is described by:

$$I_f \propto \int_0^{\infty} \phi_f(z)c(z)U_0\exp\left(-\frac{z}{\Lambda}\right)\mathrm{d}z \tag{3}$$

where ϕ_f is the fluorescence quantum efficiency of the fluorophore, $c(z)$ is the fluorophore concentration profile in the z direction, and U_0 is the fluorescence intensity at $z=0$.

Evanescent wave-induced fluorescence spectroscopy (EWIFS) (Rumbles et al. 1991) is a reasonably surface-specific method, with increased sensitivity over transmission-based techniques. This combination of the evanescent wave principle with conventional fluorescence spectroscopy (Ausserre et al. 1986; Masuhara et al. 1983) takes advantage of the inherent multidimensionality and sensitivity of fluorescence-based techniques. The process of emission yields information that is intrinsically related to the nature of the fluorophore and its immediate microenvironment (Byrne et al. 1998). EWIFS has been used to characterize the interfacial properties of many species, ranging from small dye molecules to macromolecules such as proteins, polymers, enzymes, and DNA (de Mello et al. 1997; Liebmann et al. 1991; Parsons et al. 1992; Watarai and Funaki 1996; Yao et al. 1998). The surface specificity of the evanescent wave has also been successfully used in many biosensing applications (de Mello et al. 1997).

The incorporation of time resolution into EWIFS, i.e. time-resolved evanescent wave-induced fluorescence (TREWIFS), has the potential to resolve some of the limitations of steady-state measurements since any changes in the photophysical properties of the fluorophore will be reflected in the fluorescence decay profile (Rumbles et al. 1991). Furthermore, unlike steady-state measurements in which the fluorescence quantum yield of surface adsorbed species is often assumed to be equal to that in the bulk solution (Ausserre et al. 1986), TREWIFS has the capability to detect any variation of fluorescence quantum yield as a function of distance away from the interface (de Mello et al. 1995; Rumbles et al. 1991). This can be done through varying the angle of incidence of the excitation light in order to vary the penetration depth, Λ, of the evanescent wave (see Eq. 2), i.e. variable-angle TREWIFS. Thus, when monitoring a fluorophore within an adsorbed layer, the time-resolved fluorescence decay profiles, monitored as a function of distance normal to the surface, enable depth profiling of the adsorbed species.

Variable-angle TREWIFS can be further extended to variable-angle time-resolved evanescent wave-induced fluorescence *anisotropy* measurements (EW-TRAMS), a technique well suited to the study of fluorescence depolarizing processes whose dynamics occur on the nanosecond and sub-nanosecond time scales, such as chromophore/segmental rotation, energy migration, etc. Through these measurements, it is, in principle, possible to monitor the motion of macromolecular species as a function of distance normal to an interface. For a species in bulk solution, the fluorescence decay profile from a fluorophore is monitored, following excitation with vertically polarized light, through polarizers set parallel and perpendicular to the polarization of the excitation light, i.e. $I_{VV}(t)$ and $I_{VH}(t)$ respectively. The time-resolved fluorescence anisotropy function, $r(t)$ (Eq. 4), contains information on the motion of the fluorophores on the time scale of the lifetime of the excited state:

$$r(t) = \frac{I_{VV}(t) - I_{VH}(t)}{I_{VV}(t) - 2I_{VH}(t)} \quad (4)$$

If the photo-excitation is achieved via a penetrating evanescent field, it is possible to study chromophore motion within the interfacial region, which can provide information on the binding (through rotational dynamics) of an adsorbate at an interface. Furthermore, such binding can be monitored as a function of distance from the interface simply by varying the penetration depth, Λ, of the field by changing the angle of incidence of the excitation light relative to the interface, or the wavelength of the excitation light, or the refractive index of one of the media forming the interface (Eq. 2). There is vast potential for TRAMS coupled with variable-angle evanescent wave excitation to provide spatial information on the fluorescence depolarizing processes near an interface; however, to date this has been underexploited.

Whilst TRAMS methods are well established for studying species in bulk solution, the situation is far more complex following evanescent wave excitation of interfacial species. Firstly, the intensity of emission from an oriented dipole at a dielectric interface is represented by a radial distribution function (Burghardt and Thompson 1984; Hellen and Axelrod 1987), as shown in Fig. 2 for dipoles oriented parallel or perpendicular to a silica/water interface. Furthermore, while propagating light can be polarized with respect to two orientations, within the evanescent (standing) wave, a component of the E-field exists in each of the three directions. While the penetration depth, Λ, is polarization independent (Edwards et al. 1989), the energy density at $z = 0$, E_0, depends on the polarization of the incident light. The expressions for E_0 for polarizations perpendicular, *s*, and parallel, *p*, to the plane of incidence, are, respectively:

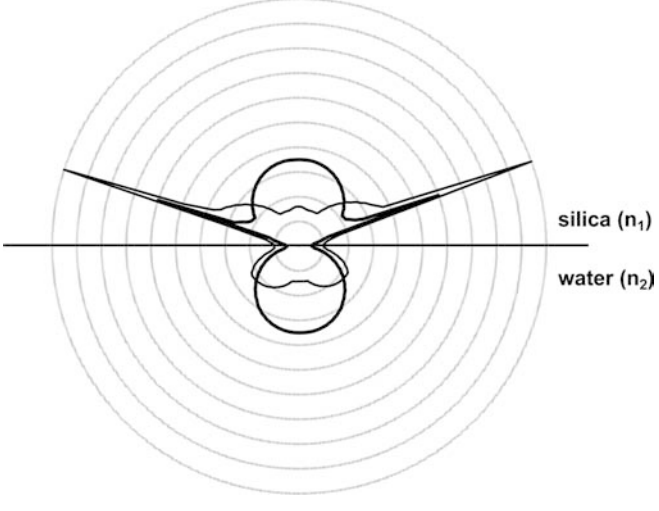

Fig. 2 Radial intensity distribution of emission dipoles parallel (*heavy solid line*) and perpendicular (*light solid line*) to a silica/water interface. n_1 and n_2 are the refractive indices of water and silica, respectively

$$E_0^s(\theta_i) = \frac{4\cos^2\theta_i}{(1 - n_{21}^2)} \quad (5)$$

$$E_0^p(\theta_i) = \frac{4\cos^2\theta_i\left[2\sin^2\theta_i - n_{21}^2\right]}{\left(n_{21}^4 cos^2\theta_i + \sin^2\theta_i - n_{21}^2\right)} \quad (6)$$

where $n_{21} = \sin\theta_c = n_2/n_1$.

Assuming that the interface is oriented vertically, vertical excitation corresponds to *s* polarization and horizontal excitation corresponds to *p* polarization. When the evanescent wave is *p* polarized, it simultaneously excites dipoles oriented both parallel and perpendicular to the interface (Harrick 1967). This complicates anisotropy measurements of rotational motion, since both emission dipole orientations are detected simultaneously. In addition, the interface itself is known to affect the emission polarization behaviour of a fluorophore, as discussed elsewhere (Lukosz 1979; Lukosz and Kunz 1977a, 1977b; Piasecki and Wirth 1994; Wirth and Burbage 1991). These effects can be corrected for by detecting emission normal to the interface with varied excitation polarization (Piasecki and Wirth 1994; Wirth and Burbage 1991).

Duplicate experiments, in which *s* and *p* polarized excitation light is used and all four permutations of the excitation and emission polarization orientations (I_{VV}, I_{VH}, I_{HV}, and I_{HH}) are collected can provide a great deal of additional information. (Note that for I_{xy}, x corresponds to the polarization of the excitation radiation and y corresponds to the orientation of the emission polarization.) Clearly, there is vast potential for TRAMS coupled with variable-angle evanescent wave excitation to provide spatial information on the fluorescence depolarizing processes near an interface (Fukumura and Hayashi 1990; Piasecki and Wirth 1994; Rumbles et al. 1994; Wirth 1993; Wirth and Burbage 1991).

In this paper we show that variable-angle TREWIFS coupled with EW-TRAMS can be used to gain information regarding the molecular conformation of a protein at an interface. To illustrate this, we investigate the rotational dynamics and molecular conformation of bovine serum albumin (BSA) adsorbed from aqueous solution onto a silica surface, in situ, and as a function of distance normal to the solid/solution interface. Additionally, we report preliminary results of the excitation polarization dependence on the time-resolved fluorescence anisotropy profiles. The time-resolved fluorescence decay and protein rotational dynamics behaviour were probed using 1-anilinonaphthalene-8-sulfonic acid (ANS), which is a fluorescent probe whose fluorescence decay kinetics depend on the probe's microenvironment such that, in a polar microenvironment, the fluorescence is rapidly and efficiently quenched. ANS associates with BSA non-covalently by partitioning into hydrophobic pockets within the

protein's tertiary structure, where the fluorescence decay of the probe is long lived.

Materials and methods

Instrumentation

The EWIFS apparatus was constructed in-house according to the arrangement shown in Fig. 3 and based on the hemi-cylindricalprism designs reported previously (de Mello et al. 1997; Hamai et al. 1995; Rumbles et al. 1994; Toriumi and Yanagimachi 1994). This arrangement is especially useful for depth profiling experiments since this configuration leads to the incident and totally internally reflected light entering and exiting the prism normal to the surface of the cylindrical part of the prism, regardless of the angle of incidence relative to the interfacial region. Details of our experimental rig have been reported previously (Lensun et al. 2002).

The majority of the limited number of TREWIFS instruments reported have principally used the time-correlated single-photon counting (TCSPC) technique (Lakowicz 1991; O'Connor and Phillips 1984), although frequency domain detection (Lundgren et al. 1994) and the use of an image intensifier/optical multichannel analyser system have also been used (Schneckenburger et al. 2000, 2001). TCSPC is a widely used tool, with exceptional sensitivity, dynamic range, and flexibility and is ideally suited to TREWIFS and hence TCSPC was used here. The TREWIFS system used is summarized schematically in Fig. 3 and described below. The excitation source is a mode-locked titanium:sapphire laser (Coherent Mira 900F-Innova 400) operating at ~800 nm and a pulse repetition rate of 76 MHz. The output of this laser was pulse picked to ~2 MHz using a TeO_2 Bragg cell (Gooch & Housego) driven by synchronized electronics (CAMAC model CD5000), and frequency doubled to ~400 nm. The polarization of the excitation beam is changed manually using a silica double-rhomb polarization rotator to allow polarization-dependent emission decay profiles to be recorded for all permutations of excitation and emission polarization pairs, i.e. $I_{VV}(t)$, $I_{VH}(t)$, $I_{HV}(t)$, and $I_{HH}(t)$. The polarized beam was incident on the sample prism at an angle of 69.0° relative to the detection axis, as shown in Fig. 3, and focused loosely onto the interfacial region. The emission was imaged with a wide-angle telephoto camera lens (Nikon) with a polarizer (King) mounted in front. The emission, collected at a constant angle, was passed through suitable filters and onto the slit of a 1/4-metre

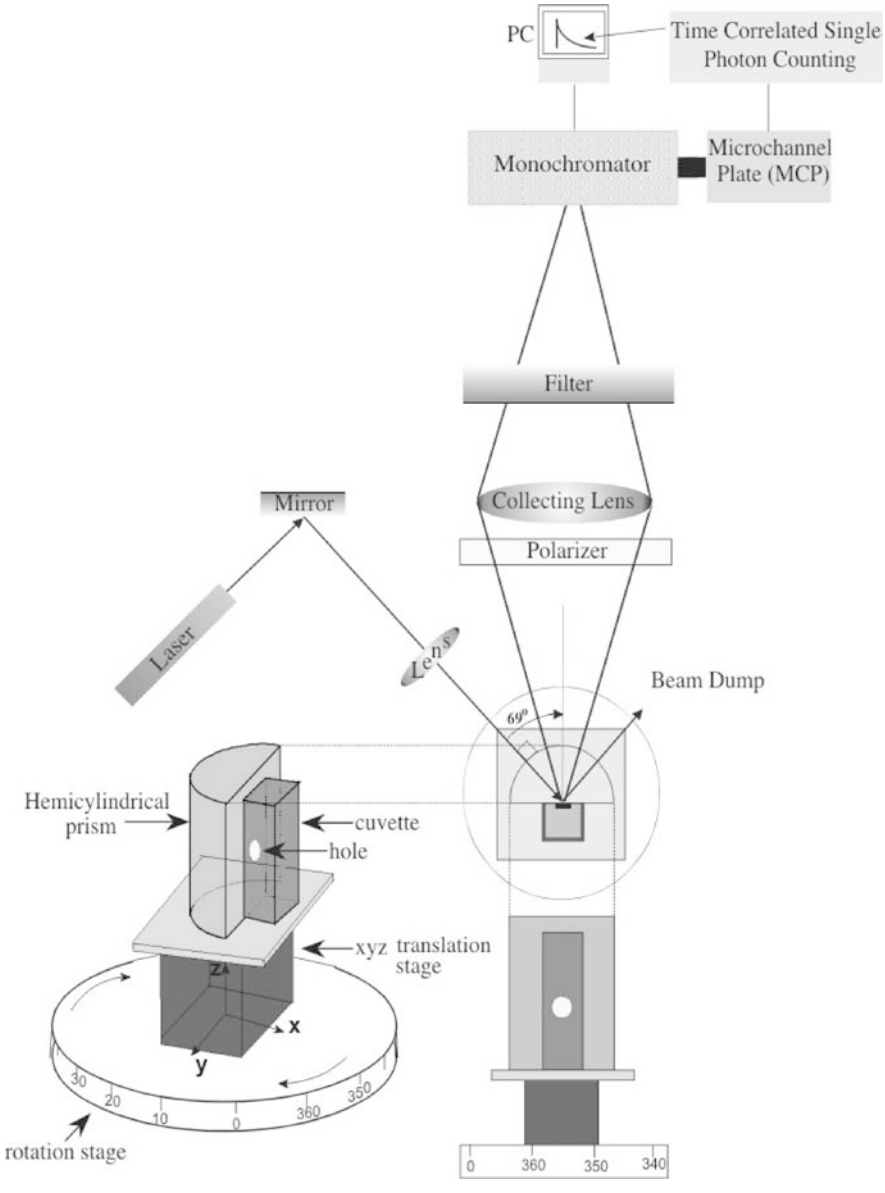

Fig. 3 Schematic representation of the in-house built EWIFS optical arrangement, used for time-resolved EWIFS and EW-TRAMS

monochromator (CVI Digikrom CM110). The fluorescence was detected by a microchannel plate photomultiplier (Eldy, St. Petersburg, Russia, model EM1-132) and recorded using conventional TCSPC electronics described elsewhere (Ghiggino and Smith 1993). Fluorescence decay data were collected to 20,000 counts at the channel of maximum intensity.

For emission anisotropy measurements, the rotatable emission polarization analyser was aligned at 0° and 90° relative to the polarized excitation to measure fluorescence decays with polarization parallel, $I_{VV}(t)$, and perpendicular, $I_{VH}(t)$, to the excitation. Data were transferred from the multichannel analyser (MCA) to a computer, where subsequent analysis of the decays was performed using non-linear least-squares iterative fitting (Smith et al. 1998). The experimentally obtained $I_{VV}(t)$ and $I_{VH}(t)$ decays were used to generate the time-resolved anisotropy, $r(t)$, function (Eq. 4). The instrumental correction factor, G, which is usually included to take into account the bias of the detector system (in particular due to the monochromator) to the polarization, was not determined here, and assumed to equal unity.

Materials and cleaning methods

Prior to each experiment, the hemi-cylindrical prism was cleaned by washing in a warm ammonia/peroxide solution, as previously described, then rinsed with MilliQ water.

All of the chemical reagents were used without any further purification. The BSA and ANS were purchased from Sigma. The solvent used was a 0.01 M acetate buffer solution, giving a pH of 5. All experiments were carried out at room temperature (approx. 20 °C), following an equilibration time of approximately 3 h.

Experimental protocols

The spectroscopic absorption and emission of ANS and BSA-bound ANS in bulk solution were characterized using a Varian Cary 50 Bio steady-state absorption spectrometer and a Cary Eclipse fluorimeter, respectively. Emission spectra were background subtracted and corrected for detector and monochromator response. The excitation wavelength was 385 nm and emission was scanned between 400 nm and 600 nm. The excitation and emission bandwidths were set to 2.5 nm and the PMT voltage was set to 800. Steady-state measurements were performed using ANS at a constant concentration of 1×10^{-5} M as a function of different BSA concentrations, varying from 10 to 100 ppm.

For the TREWIFS and EW-TRAMS, solutions of ANS and BSA (BSA concentration ~100 ppm) were prepared in buffered solution (pH 5) and were allowed to be adsorbed from solution to the silica surface for 3 h, after which it was assumed that adsorption was complete and that the fluorescence decay can be observed with little variation.

TREWIFS experiments were carried out as a function of angle of incidence to allow depth profiling of the protein via the probe's fluorescence. Two sets of experimental conditions were used, referred to as type A and type B. Type A measurements were performed on BSA-ANS adsorbed from solution, maintaining equilibrium with BSA-ANS in the bulk. A set of fluorescence decay profiles was obtained for a variety of angles of incidence ranging from 69° to 89° with 4° increments. Hence, the penetration depth ranged from 100 nm to 40 nm (Eq. 2). The type B measurements were performed after the bulk solution of BSA-ANS had been replaced by thorough flushing of the cell with acetate buffer solution to remove any non-adsorbed or loosely adsorbed BSA. This procedure ensured that the silica surface was always in contact with aqueous solution. Once the protein solution was replaced with the buffer, emission decays were taken at the angles of incidence specified above. The EW-TRAMS experiment was carried out also as a function of penetration depth of the evanescent wave.

To characterize the anisotropy of non-adsorbed BSA, TRAMS were also performed in bulk solution with the sample solution contained in a standard silica quartz cuvette and the emission collected in the usual right-angle geometry. A full description of the instrumentation used for the bulk measurements is given elsewhere (Smith et al. 1998).

Results and discussion

It is well documented that neither unbound ANS nor BSA alone fluoresce significantly in buffered aqueous solution under the excitation and emission wavelengths used here ($\lambda_{exc}\approx390$ nm, $\lambda_{em}\approx490$ nm). When no BSA is present, no hydrophobic regions exist into which the ANS can partition, and the emission of ANS is quenched very efficiently. This can be easily resolved from the intrinsic fluorescence of BSA, which fluoresces around 344 nm in bulk solution and ~333 nm in close proximity to surfaces (Hlady and Andrade 1988), when following direct excitation in the ultraviolet of the amino acids, especially tryptophan.

When the fluorescence of BSA-bound ANS is measured, it is observed that as the concentration of BSA in bulk solution is increased, the fluorescence quantum yield of the ANS increases dramatically. This is a direct result of the increase in the number of hydrophobic regions per unit volume as more BSA is added to solution, thus protecting the ANS from the fluorescence quenching mechanism in aqueous environments. There is negligible spectral shift of the ANS emission profile upon complexation with the protein or upon the adsorption of the BSA-ANS complex to the silica surface.

TREWIFS measurements in variable-angle mode have the capacity to yield information on the conformation of a protein at an interface. To illustrate this, TREWIFS measurements were recorded from the silica-adsorbed BSA-ANS complex as a function of excitation angle relative to the interface (and hence penetration depth), as previously reported (Lensun et al. 2002). The TREWIFS results are shown in Fig. 4 ($\lambda_{exc}=400$ nm, $\lambda_{em}\approx 470$ nm). In type A measurements, the fluorescence decay profiles were measured from the surface-adsorbed BSA-ANS complex adsorbed from buffered bulk solution. At the highest angle of incidence employed, the depth of the penetration (i.e. $\Lambda=40$ nm) will still be longer than the thickness of the interfacial region. Therefore, in these measurements, the fluorescence intensity will not only have a contribution from the surface region, but will also contain a significant proportion of emission from any free BSA-ANS complex remaining in bulk solution (referred to as "bulk" in Fig. 4). In type B measurements, however, non-adsorbed and any reversibly adsorbed protein was slowly flushed out of the cell. Even though the evanescent field penetrates beyond the interfacial region, the bulk buffer solution will not contribute to the fluorescence intensity. Hence, in type B measurements, the fluorescence decays comprise solely the signal from the surface-adsorbed form of the BSA-ANS complex (referred to as "surface" in Fig. 4). The decay profiles were significantly different to those of the bulk solution and these decays were

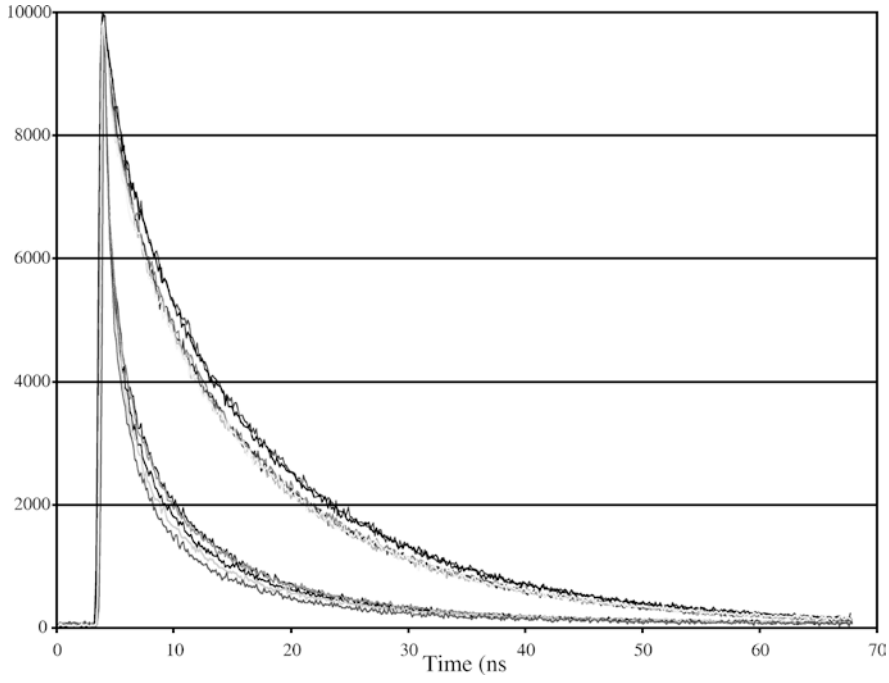

Fig. 4 Time-resolved fluorescence decay curves of the BSA-ANS complex as a function of penetration depth, Λ, of the evanescent wave normal to the interface. Two data sets are presented, corresponding to type A and to type B experimental protocols, as described in Materials and methods. The penetration depth was varied from around 40 nm to around 100 nm in 12 nm intervals, within each data set

reproducible over several hours, indicating that the remaining BSA is, indeed, irreversibly adsorbed.

It is difficult and often misleading to assign any physical significance to the individual components of a multi-exponential fit to the fluorescence decay. Instead, we compare the relative total emission quantum yield of each of the decay profiles. Differences between the fluorescence quantum yield of BSA-ANS in the bulk solution and that of BSA-ANS near the surface are clearly observed by a significant shortening of the fluorescence decay curves recorded at shallower penetration depths as compared with those recorded from the bulk solution. The decay curves collected under type B conditions show that the fluorescence decay is most rapid when the penetration depth, Λ, is smallest. This implies that ANS within the adsorbed layer experiences a more polar microenvironment the closer the ANS is to the silica surface.

Assuming that k_r, the radiative deactivation rate coefficient, is independent of environment, then Eq. (3) above can be rewritten as:

$$I_f = k_r \int_0^{\infty} \tau_f(z) c(z) U_0 \exp\left(-\frac{z}{\Lambda}\right) dz \qquad (7)$$

suggesting that a distribution of decay times might be a more appropriate model for interpreting the fluorescence decay profiles, rather than a sum of a discrete number of exponential terms. This was not attempted in this work, but we are currently working on a method by which a fluorescence decay profile can be fitted to a distribution of decay times so as to gain more detailed quantitative information on how the macromolecular conformation varies with distance from the interface. We plan to present some of this work in a future publication.

The change in fluorescence decay observed as a function of incident angle under the "bulk" (type A) conditions is attributed to the contributions in quantum yield variation from the surface-adsorbed species inherent in the decays of the bulk.

The adsorption of BSA onto silica has been investigated in detail previously by EWIFS methods using the intrinsic fluorescence of BSA (Rainbow et al. 1987) and a variety of fluorescence probes, including ANS (Burghardt and Axelrod 1983; Crystall et al. 1993; Fukumura and Hayashi 1990; Hlady and Andrade 1988, 1989; Suci and Hlady 1990). The behaviour of ANS itself near interfaces has also been investigated (Bessho et al. 1997; Hlady et al. 1988). The work to date has indicated that, upon adsorption to silica, BSA undergoes some degree of conformational change (Burghardt and Axelrod 1983; Rainbow et al. 1987). Hlady and colleagues (Hlady and Andrade 1988, 1989; Suci and Hlady 1990) have presented data that indicate the presence of some sort of surface aggregates at high BSA surface concentrations, in agreement with the existence of two-dimensional aggregates of adsorbed BSA concluded by others. These authors also interpret a change in the distance between energy donors and acceptors as being due to conformational changes (partial unfolding of adsorbed BSA) upon adsorption (Hlady and Andrade 1989). Fukumura and Hayashi (1990) also reported that BSA undergoes conformational change upon adsorption to a silica surface. In addition, Hlady and Andrade (1988) reported that the conformation change involves the tryptophan group of BSA becoming embedded further within more hydrophobic regions of the coil, while the ANS probe groups experience a more polar environment (hence fluorescence quenching) through increased exposure to more hydrophilic regions.

Our time-resolved fluorescence decay results, that illustrate a hydrophobicity gradient in the adsorbed layer normal to the surface, are also consistent with the existence of a conformational change of BSA upon adsorption to the silica interface. We provide here the additional information regarding the dependence of the fluorescence decay on penetration depth of the evanescent field, Λ. This allows the conformation of the adsorbed protein to be resolved spatially, normal to the surface. The observed decrease in fluorescence quantum efficiency at small Λ may be explained by the BSA unfolding, thus exposing bound ANS groups to a more polar environment than that experienced by the BSA-ANS complex in bulk solution. It appears that BSA unfolds to the greatest extent at the silica surface so as to optimize its interaction with silica, since, further away from the silica surface (as Λ increases), there is a corresponding increase in fluorescence decay time. This indicates that, further away from the silica surface, an adsorbed BSA molecule is increasingly more coiled and so retains increasingly more hydrophobic sites where ANS resides.

The difficulties in analysing fluorescence decay profiles of fluorophores near surfaces are well documented and, until further work in this area definitively solves this problem, the value of fluorescence decays per se may be limited. Nonetheless, it is clear that time-resolved measurements are more informative than steady-state measurements alone. Fluorescence anisotropy measurements, while also suffering from drawbacks such as poorer signal quality and complexity of analysis, have the potential to provide additional qualitative and quantitative information on dynamic processes that can contribute to a loss of emission polarization, including energy transfer, migration, and fluorophore/segmental rotation motion. Evanescently induced TRAMS (EW-TRAMS) should aid in identifying whether the changes observed in the fluorescence decay profiles of BSA-ANS as a function of penetration depth are in fact related to partial denaturation of the protein upon adsorption, thus exposing the ANS to more aqueous environments.

EW-TRAMS measurements on the surface-adsorbed BSA-ANS complex were conducted as a function of penetration depth, under the type B conditions discussed above. The resulting time-resolved fluorescence anisotropy profiles from these experiments are shown in Fig. 5. It is clear from these data that as the depth of penetration of the evanescent wave is reduced, the fluorescence anisotropy decays far more slowly than is the case in bulk solution. This indicates that as the protein adsorbs onto the surface, the motion of the parts of the protein to which the ANS is bound are more restricted, as might be expected. This suggests that not only is the BSA coil as a whole undergoing restricted rotation, but also the more rapid segmental motion of the ANS-bound segments of the protein is severely hindered. This corroborates the interpretation of the EWIFS data, discussed above. The shortening of the fluorescence decay profiles observed (Fig. 4) does not appear to be the result of a simple opening up of the BSA coil conformation on adsorption, since this might be expected to increase the time-scale of the motion of the individual ANS-bound BSA segments, rather than decrease it as observed. One mechanism by which these observations may be explained is an unravelling of the BSA coil at the silica surface, leading to an increase in the number of points of attachment. Any ANS bound to portions of the BSA that experience this uncoiling and adsorption to the surface will consequently exhibit restricted rotation due to the inhibited coil and chain segment motion. This restriction of the chromophore motion supports the findings discussed above relating to the TREWIFS measurements.

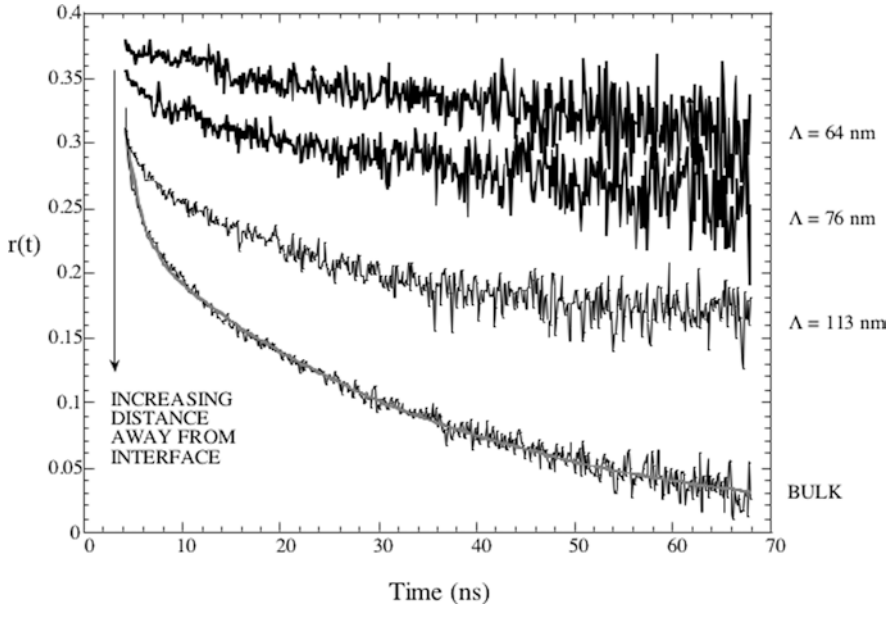

Fig. 5 Time-resolved fluorescence anisotropy profiles of the BSA-ANS complex recorded as a function of depth penetration, Λ, of the evanescent wave

It is well known that fluorescence anisotropy decays can become very complex to analyse even for relatively simple systems (Smith et al. 1998), and often the quality of the data does not justify the use of complex analysis functions. As discussed above, fluorescence anisotropy measurements are further complicated under EWIFS conditions (Rumbles et al. 1994). In light of these complications, in this work, the time-dependent fluorescence anisotropy decays have not been analysed analytically, but rather qualitatively at this stage. Another possible complication arises if the adsorbed species is not isotropic, as discussed above and illustrated in Fig. 2. Certain adsorbed species might exhibit spatial alignment relative to the surface leading to anisotropy of the absorption and emission dipole moments (Wirth 1993; Wirth and Burbage 1991). Assuming a vertically oriented interface (e.g. Fig. 3), by using both *s* and *p* polarized evanescent wave excitation (as discussed above), rotational motion can be investigated in two planes, i.e. in and out of the plane of the interface.

In principle, monitoring anisotropy following excitation by both *s* (vertically) and *p* (horizontally) polarized incident light yields information relating to motion of fluorophores with emission dipoles oriented both in and out of the plane of the interface (Piasecki and Wirth 1994; Wirth and Burbage 1991), i.e. molecular motion in two orthogonal planes can be identified, as illustrated schematically in Fig. 6.

The definitions of anisotropy are based on intensity ratios of a number of combinations of polarization (Wirth and Burbage 1991):

$$\text{Bulk}: \quad r_{\text{bulk}} = \frac{I_{\text{VV}} - I_{\text{VH}}}{I_{\text{VV}} - 2I_{\text{VH}}} \tag{8}$$

$$\text{In}-\text{plane}: \quad r_{\phi} = \frac{I_{yy} - I_{yx}}{I_{yy} + I_{yx}} \tag{9}$$

$$\text{Out}-\text{of}-\text{plane}: \quad r_{\theta} = \frac{I_{zy} - \frac{1}{2}\left(I_{yy} + I_{yx}\right)}{I_{zy} + I_{yy} + I_{yx}} \tag{10}$$

Preliminary results from excitation polarization-dependent time-resolved fluorescence anisotropy measurements for the BSA-ANS system with a penetration depth of ~64 nm are presented in Fig. 7. There is a clear difference between the decay of the anisotropy profiles corresponding to the in- and out-of-plane motion (Eqs. 9 and 10, respectively) of the fluorophore. The decay of the fluorescence anisotropy is related to the rate of reorientation of the emission dipoles. The data shown clearly indicate that motion is more rapid in the plane of the interface than orthogonal to it. This represents, to our knowledge, the first example of an excitation polarization-dependent time-resolved fluorescence anisotropy measurement and illustrates the potential of this approach to spatially resolving two-dimensional motion of fluorophores near an interface.

Conclusions

We have shown that variable-angle, time-resolved, evanescent wave-induced fluorescence decay measurements and EW-TRAMS can be applied to the study of adsorption-induced protein denaturation and that TREWIFS and EW-TRAMS are able to monitor protein molecular conformational changes normal to the surface. Specifically, we have successfully studied the extent to which BSA denatures upon adsorption at a silica surface, using ANS as a fluorescent probe. When adsorbed, BSA adopts a more "open" structure through which it exposes the BSA-ANS binding sites to a slightly more hydrophilic environment (including the silica surface). The shortening of the fluorescence decay as the emission closer to the interface is probed (Fig. 4) is most likely due to a slight decrease in hydrophobicity experienced by the ANS as the protein denatures. The variation of fluorescence quantum yield with distance from the interface suggests a hydrophobicity gradient experienced by the ANS in the region of the interface. The EW-TRAMS show an increase in the overall time-scale of the motion of the protein segments to which the ANS is bound as the emission is probed from closer to the interface. The results are consistent with a model of partial protein denaturation: at the surface, an adsorbed BSA molecule unfolds, thus optimizing protein–silica interactions and the number of points of attachment to

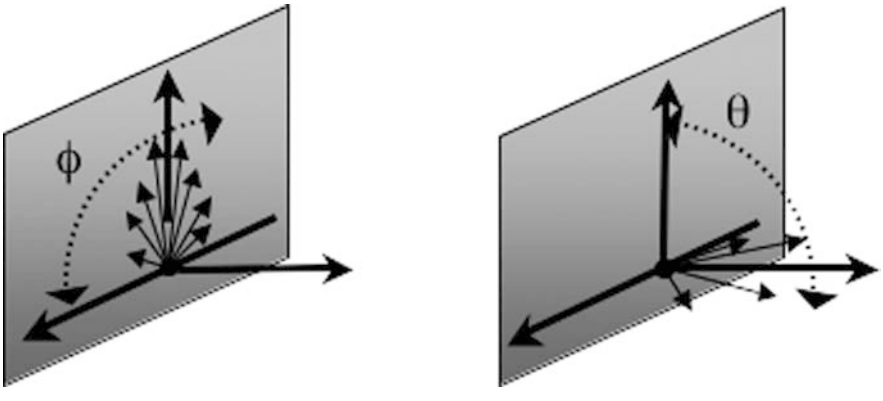

Fig. 6 Schematic diagram of the in- and out-of-plane rotations of an emission dipole at an interface

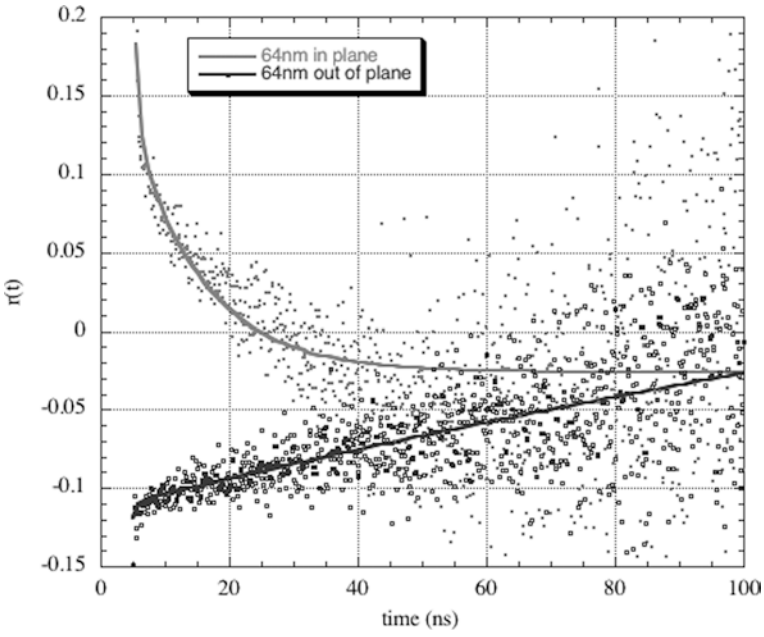

Fig. 7 Excitation polarization-dependent, time-resolved fluorescence anisotropy decay profiles recorded for BSA-ANS adsorbed onto silica, illustrating differences in the rate of in- and out-of-plane motion. The penetration depth is ~64 nm

the surface. Further away, normal to the surface, the protein molecule maintains its coiled structure.

Acknowledgements The authors would like to thank Professor Ken Ghiggino for providing access to the laser equipment. We also acknowledge the Australian Research Council for their generous financial support of the work in the form of an ARC Large Grant.

References

Ausserre D, Hervet H, Rondelez F (1986) Concentration dependence of the interfacial depletion layer thickness for polymer solutions in contact with nonadsorbing walls. Macromolecules 19:85–88

Bessho K, Uchida T, Yamauchi A, Shioya T, Teramae N (1997) Microenvironments of 8-anilino-1-naphthalenesulfonate at the heptane-water interface: time-resolved total internal reflection fluorescence spectroscopy. Chem Phys Lett 264:381–386

Burghardt TP, Axelrod D (1983) Total internal reflection fluorescence study of energy transfer in surface-adsorbed and dissolved bovine serum albumin. Biochemistry 22:979–985

Burghardt TP, Thompson NL (1984) Effect of planar dielectric interfaces on fluorescence emission and detection. Evanescent excitation with high-aperture collection. Biophys J 46:729–737

Byrne CD, de Mello AJ, Barnes WL (1998) Variable-angle time-resolved evanescent wave-induced fluorescence spectroscopy (VATR-EWIFS): a technique for concentration profiling fluorophores at dielectric interfaces. J Phys Chem B 102:10326–10333

Cornelius RM, Brash JL (1999) Adsorption from plasma and buffer of single- and two-chain high molecular weight kininogen to glass and sulphonated polyurethane surfaces. Biomaterials 20:341–250

Crystall B, Rumbles G, Smith TA (1993) Time resolved evanescent wave induced fluorescence measurements of surface adsorbed bovine serum albumin. J Colloid Interface Sci 155:247–250

de Mello AJ, Crystall B, Rumbles G (1995) Evanescent wave spectroscopic studies of surface enhanced fluorescence quantum efficiencies. J Colloid Interface Sci 169:161–167

de Mello AJ, Elliott JA, Rumbles G (1997) Evanescent wave-induced fluorescence study of rhodamine 101 at dielectric interfaces. J Chem Soc Faraday Trans 93:4723–4731

Edwards J, Ausserre D, Hervet H, Rondelez F (1989) Quantitative studies of evanescent wave intensity profiles using optical fluorescence. Appl Opt 28:1881–1884

Fukumura H, Hayashi K (1990) Time-resolved fluorescence anisotropy of labelled plasma proteins adsorbed on polymer surfaces. J Colloid Interface Sci 135:435–442

Ghiggino KP, Smith TA (1993) Dynamics of energy migration and trapping in photoirradiated polymers. Prog React Kinet 18:375–436

Hamai S, Tamai N, Masuhara H (1995) Excimer formation of pyrene in a solid/polymer solution interface layer. A time-resolved total internal reflection fluorescence study. J Phys Chem 99:4980–4985

Harrick NJ (1967) Internal reflection spectroscopy. Wiley-Interscience, New York

Hellen EH, Axelrod D (1987) Fluorescence emission at dielectric and metal-film interfaces. J Opt Soc Am B 4:337–350

Hlady V, Andrade JD (1988) Fluorescence emission from adsorbed bovine serum albumin and albumin-bound 1-anilinonaphthalene-8-sulfonate studied by TIRF. Colloids Surf 32:359–369

Hlady V, Andrade JD (1989) A TIRF titration study of 1-anilinonaphthalene-8-sulfonate binding to silica-adsorbed bovine serum albumin. Colloids Surf 42:85–96

Hlady V, Gölander C, Andrade JD (1988) Hydrophobicity gradient on silica surfaces: a study using total internal reflection fluorescence spectroscopy. Colloids Surf 33:185–190

Lakowicz JR (1991) Topics in fluorescence spectroscopy, vols 1–3. Plenum Press, New York

Lensun L, Smith TA, Gee ML (2002) The partial denaturation of silica-adsorbed bovine serum albumin determined by time-resolved evanescent wave-induced fluorescence spectroscopy. Langmuir 18:9924–9931

Liebmann LW, Robinson JA, Mann KG (1991) A dual beam total internal reflection fluorescence spectrometer for dynamic depth resolved measurements of biochemical liquid-solid Interface binding reactions in opaque solvents. Rev Sci Instrum 62:2083–2092

Lukosz W (1979) Light emission by magnetic and electric dipoles close to a plane dielectric interface. III. Radiation patterns of dipoles with arbitrary orientation. J Opt Soc Am 69:1495–1503

Lukosz W, Kunz RE (1977a) Light emission by magnetic dipoles close to a plane interface. I. Radiation patterns of perpendicular oriented dipoles. J Opt Soc Am 67:1615

Lukosz W, Kunz RE (1977b) Light emission by magnetic dipoles close to a plane interface. I. Total radiated power. J Opt Soc Am 67:1607–1614

Lundgren JS, Bekos EJ, Wang R, Bright FV (1994) Phase-resolved evanescent wave induced fluorescence. An in situ tool for studying heterogeneous interfaces. Anal Chem 66:2433–2440

Masuhara H, Mataga N, Tazuke S, Murao T, Yamazaki I (1983) Time-resolved total internal reflection fluorescence spectroscopy of polymer films. Chem Phys Lett 100:415–419

O'Connor DV, Phillips D (1984) Time correlated single photon counting. Academic Press, London

Parsons D, Harrop R, Mahers EG (1992) The kinetics of particle and polymer adsorption by total internal reflection fluorescence. Colloids Surf 64:151–160

Piasecki DA, Wirth MJ (1994) Spectroscopic probing of the interfacial roughness of sodium dodecyl sulfate adsorbed to a hydrocarbon surface. Langmuir 10:1913–1918

Rainbow MR, Atherton S, Eberhart RC (1987) Fluorescence lifetime measurements using total internal reflection fluorimetry: evidence for a conformational change in albumin adsorbed to quartz. J Biomed Mat Res 21:539–555

Ratner BD (1989) In: Aggarwal S (ed) Comprehensive polymer science: the synthesis, characterization, reactions and applications of polymers, vol 7. Pergamon Press, Oxford, pp 201–247

Rumbles G, Brown AJ, Phillips D (1991) Time-resolved evanescent wave induced fluorescence spectroscopy, part 1. Deviations in the fluorescence lifetime of tetrasulphonated aluminium phthalocyanine at a fused silica/methanol interface. J Chem Soc Faraday Trans 87:825–830

Rumbles G, Bloor D, Brown AJ, de Mello AJ, Crystall B, Phillips D, Smith TA (1994) Time-resolved evanescent wave induced fluorescence studies of polymer-surface interactions. In: Masuhara H, Schryver FCD, Kitamura N, Tamai N (eds) Microchemistry: spectroscopy and chemistry in small domains. Elsevier, London, pp 269–286

Schneckenburger H, Stock K, Eickholz J, Strauss WSL, Lyttek M, Sailer R (2000) Time-resolved total internal reflection fluorescence spectroscopy: application to the membrane marker laurdan. In: König K, Tanke HJ, Schneckenburger H (eds) Proc SPIE, laser microscopy, vol 4164. SPIE, Amsterdam, Netherlands, pp 36–42

Schneckenburger H, Sailer R, Stock K, Lyttek M, Strauss WSL (2001) Total internal reflection fluorescence lifetime imaging (TIR-FLIM) of living cells. In: Gu M (ed) Multidimensional microscopy 2001, 3rd Asia–Pacific international symposium on confocal microscopy and related technologies, Melbourne, Australia, p 65

Smith TA, Irwanto M, Haines DJ, Ghiggino KP, Millar DP (1998) Time-resolved fluorescence anisotropy measurements of the adsorption of rhodamine-B and a labelled polyelectrolyte onto colloidal silica. Colloid Polym Sci 276:1032–1037

Suci P, Hlady V (1990) Fluorescence lifetime components of Texas Red-labelled bovine serum albumin: comparison of bulk and adsorbed states. Colloids Surf 51:89–104

Toriumi M, Yanagimachi M (1994) Time-resolved total-internal reflection fluorescence spectroscopy and its applications to solid/polymer interface layers. In: Masuhara H, Schryver FCD, Kitamura N, Tamai N (eds) Microchemistry: spectroscopy and chemistry in small domains. Elsevier, London, pp 257–268

Watarai H, Funaki F (1996) Total internal reflection fluorescence measurements of protonation equilibria of rhodamine B and octadecylrhodamine B at a toluene/water interface. Langmuir 12:6717–6720

Wirth MJ (1993) Magic angle lifetime measurements in evanescent wave fluorometry. Appl Spectrosc 47:651–653

Wirth MJ, Burbage JD (1991) Adsorbate reorientation at a water/(octadecylsilyl)silica interface. Anal Chem 63:1311–1317

Yao H, Ikeda H, Kitamura N (1998) Surface-induced aggregation of pseudoisocyanine dye at a glass/solution interface studied by total-internal reflection fluorescence spectroscopy. J Phys Chem 102:7691–7694